

Modeling of inner plasma sheet and ring current during substorms

Mei-Ching Fok

Universities Space Research Association, NASA Goddard Space Flight Center, Greenbelt, Maryland

Thomas E. Moore

Interplanetary Physics Branch, NASA Goddard Space Flight Center, Greenbelt, Maryland

Dominique C. Delcourt

Centre d'étude des Environnements Terrestre et Planétaires, Saint-Maur des Fosses, France

Abstract. The evolution of the inner plasma sheet and the ring current during substorm dipolarizations is simulated. A substorm cycle is treated by stretching and dipolarizing the magnetosphere according to the Tsyganenko 89 model. In order to clarify the relative influences of steady convection and induction electric field on ring current development, the inductive electric field is superposed on two baseline convective states: a nonstorm state using a weak electric field, and a storm-time state using a stronger electric field. Ion distributions on the nightside at 12 Earth radii (R_E) during these two substorms are obtained using our single-particle code to trace particle trajectories backward in time to source regions assumed to have steady characteristics. The subsequent acceleration and transport of these boundary ions into the inner magnetosphere is modeled by our kinetic model of the ring current. The simulation generates many frequently observed features of substorm injections, including the sudden appearance of hot plasma tailward of a sharply defined "injection boundary," the earthward motion of an "injection front," the azimuthal and tailward expansion of this enhanced region, and the creation of characteristic ion dispersion patterns near geosynchronous orbit. Comparison of the nonstorm and storm cases suggests that substorms occurring without a convection enhancement produce mainly an enhancement of the cross-tail current but little change in the ring current. With strong convection, the role of substorms is to enable the convection enhancement to create robust ring current in the inner magnetosphere.

1. Introduction

By now it is reasonably well established that the terrestrial ring current is carried by plasmas that are injected from the inner plasma sheet through the nightside geosynchronous orbit region [Wolf *et al.*, 1997; Fok *et al.*, 1996]. Particle acceleration and heating are known to accompany this process, but the nature of the plasma flows and electromagnetic fields responsible for it remain somewhat indeterminate and controversial. On the one hand, enhanced global convection has been shown to be capable of generating a credible ring current through a number of simulation efforts [Harel *et al.*, 1981; Wolf *et al.*, 1997]. On the other hand, large and very rapid changes in the nightside magnetic field induce strong electric fields that are well known and highly visible features of magnetospheric substorms [McIlwain, 1974; Aggson and Heppner, 1977; Shepherd *et al.*, 1980; Moore *et al.*, 1981; Arnoldy and Moore, 1983; Mauk and Meng, 1983, 1986; Lopez and Lui, 1990]. The main phase of magnetospheric storms often gives the appearance of a rapid succession of substorms, each consisting of a cycle of

magnetotail distention and dipolarization. Indeed, this is the semantic basis for the term "substorm." At one time, the induced electric fields associated with substorms were thought to be so important that it has been suggested that they are responsible for all transport of plasma from the plasma sheet into the inner magnetosphere [Mauk and Meng, 1983; B. Mauk, private communication, 1983].

Recently, however, some evidence has developed that individual substorms may be somewhat incidental to the main phase of a storm [Gonzalez *et al.*, 1994; Chen *et al.*, 1994]. The argument is that cycles of distention and dipolarization have no net effect on the transport of plasma, with all net plasma transport into the inner magnetosphere being accomplished by enhanced global convection electric fields. Chen *et al.* [1994] used spike-like enhancements of the convection electric field to simulate the effect of individual substorms. Fok *et al.* [1996] used an inductive, localized electric field tied to cycles of stretching and dipolarization of the Tsyganenko magnetic field model in a ring current modeling effort. The results suggested that substorms may actually hinder the development of a ring current until they are overwhelmed by strong global convection.

Nevertheless, interest in the induced electric fields characteristic of highly disturbed periods remains very strong [Li *et al.*, 1993; Birn *et al.*, 1997], and it seems likely that

Copyright 1999 by the American Geophysical Union.

Paper number 1999JA900014.

0148-0227/99/1999JA900014\$09.00

they somehow play an important role in accelerating storm-time particles. *Liu and Rostoker* [1995] considered a series of recurring substorms and concluded that nonadiabatic dynamics of charged particles serve as a catalyst for long-term energization. A lingering controversy centers around the spatial propagation of substorm dipolarization disturbances, with works by *Lopez et al.* [1988, 1990] indicating that dipolarization and particle acceleration signatures actually propagate tailward from the geosynchronous orbit region, rather than earthward as found by *Moore et al.* [1981]. More recently, other works [*Jacquey et al.*, 1993; *Ohtani*, 1998] have also observed apparent earthward propagation of substorm effects in the region near and inside geosynchronous orbit. Moreover, *Li et al.* [1998] have recently shown that propagating dipolarization signals have effects that help to explain the acceleration of relativistic electron populations.

As we completed the *Fok et al.* [1996] study, we recognized that dipolarization effects in the magnetotail had probably been underestimated, because of the lack of a time-dependent description of the plasma present at the outer boundary of our ring current simulation, near geosynchronous orbit. Dipolarization in the tail and the breaking of adiabaticity could strongly influence the characteristics of the plasma being fed into the ring current growth region. To correct this, we sought to use the three-dimensional (3D) test particle code of D. Delcourt [*Delcourt et al.*, 1990; *Delcourt and Sauvaud*, 1994] to generate this ring current outer boundary condition as an inner boundary result for a dipolarizing plasma sheet, fed by constant sources of boundary plasmas. In this study, we report results that indicate a more prominent role for dipolarization electric fields, though the underlying global circulation remains very important in our simulations.

In particular, we are able to generate many of the features of substorm injections seen near geosynchronous orbit, including the earthward motion of an injection front, setting up an injection boundary (similar to that of *McIlwain* [1974] and *Mauk and Meng* [1983]), azimuthal expansion to earlier and later local times, and finally, the appearance of tailward expansion. In addition, the dispersive features of substorm plasma clouds in the magnetosphere [*DeForest and McIlwain*, 1971] are reproduced in the simulation at virtual spacecraft in synchronous orbit. When the near-Earth plasma sheet is simulated this way, the effects of enhanced global convection and those of individual substorm dipolarizations appear to be additive, such that the aggregate ring current is the superposition of contributions from both.

2. Evolution of the Inner Plasma Sheet During Substorms

The three-dimensional particle code of Delcourt [*Delcourt et al.*, 1990; *Delcourt and Sauvaud*, 1994] is used to calculate particle trajectories in order to set up the proton distributions on the nightside along a boundary at a constant equatorial 12 Earth radii (R_E). This test-particle code computes the guiding center equation in the near-Earth region and the full equation of particle motion at larger distance. The magnetic field is modeled by the empirical model of Tsyganenko [*Tsyganenko*, 1989], assuming zero dipole tilt angle and dipole axis normal to the Sun-Earth direction. The magnetic field is varied to simulate the magnetic reconfiguration during substorms. The electric field induced by the magnetic variation is calculated using the vector potential technique of *Delcourt et al.* [1990].

The steady convection is given by the electric field model of *Volland* [1978], with large cross-polar cap potential drop representing storm-time convection and small potential for nonstorm condition.

In this study, a substorm cycle is represented by a constant magnetic field of level 1 (corresponding to $Kp = 0, 0+$) for 15 min, then the growth phase during which the magnetosphere stretches from level 1 to level 5 (corresponding to $Kp = 4-, 4, 4+$) in 30 min. This is followed by a 10 min substorm expansion phase when the magnetic field relaxes back to dipole-like configuration (level 1). The magnetic field is then maintained at the ground level for the next 15 min. The convection electric field is assumed to be constant during this 70-minute period. A cross-polar cap potential drop (Φ_p) of 40 kV is taken to represent a nonstorm substorm (substorm 1), while a potential drop of 80 kV is chosen for storm-time substorm (substorm 2). Figure 1 depicts the time history of the magnetic field level and Φ_p during these two simulated substorms. In the top panel, t_1 , t_2 , t_3 , and t_4 correspond to the times at the beginning of the growth phase, at the onset of expansion phase, right after substorm expansion, and 15 min after expansion, respectively. According to the Tsyganenko 89 model, dipolarizing the magnetosphere from level 5 to level 1 produces a magnetic field recovery of 21 nT at the midnight geosynchronous orbit. It can be seen in Figure 1 that the magnetic field level does not rise or drop linearly during transitions. In fact, the temporal variation is fitted by a polynomial of degree 5 to ensure zero values of the inductive electric field and its time derivative at the beginning and at the end of transition [*Delcourt et al.*, 1990]. As a result, the fastest reconfiguration (largest induced electric field) occurs at the middle of each transition. In these simulations, at the middle of dipolarization, the inductive electric field is ~ 4 mV/m at the midnight geosynchronous orbit, while the steady convection field at the same position is ~ 1 mV/m for the case

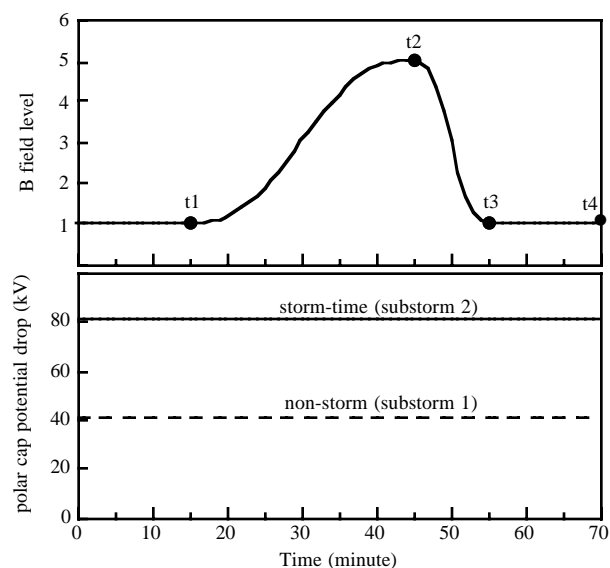


Figure 1. (top) Model magnetic field level as a function of time: t_1 , t_2 , t_3 , and t_4 corresponds to the times at the beginning of growth phase, at the onset of expansion phase, right after substorm expansion, and 15 min after expansion. (bottom) Cross-polar cap potential drop during the storm-time substorm (solid line) and the nonstorm substorm (dashed line).

Table 1. Sources of Initial Distributions in the Entire Magnetosphere.

Region	Model / Data	Reference
Ionosphere	latitude $< 60^\circ$: IRI-95	<i>Bilitza et al.</i> [1993]
	latitude $\geq 60^\circ$: IRI-95 + polar wind (polar wind: drifting Maxwellian with $v_{\parallel} = 40$ km/s, $n = 0.1$ cm $^{-3}$, $T = 1$ eV)	<i>Ganguli</i> [1996] <i>Moore et al.</i> [1997]
Inner magnetosphere ($1.1 \leq r(R_E) \leq 7.7$)	CCE/CHEM data	<i>Sheldon and Hamilton</i> [1993]
Plasma sheet, lobes	Maxwellian with n and T given by MHD simulation	<i>Hesse and Birn</i> [1998]
Plasma mantle, LLBL	Maxwellian with $n = 5$ cm $^{-3}$, $T = 300$ eV	<i>Hughes</i> [1996]

of strong convection and 0.5 mV/m for weak convection. Though the dipolarization is presumably the result of the operation of a neutral line, it is always beyond the simulation space in this approach. The same calculations could clearly be conducted in a space containing a neutral line, though we believe it would have a quantitative rather than qualitative effect.

To find the H^+ flux at a given location along the $12 R_E$ boundary, energy and pitch angle, at given time (t) during a substorm, the particle trajectory is traced backward in time from time = t to time = 0 or until the particle reaches the model boundaries at the deep magnetotail ($70 R_E$), plasma mantle, low-latitude boundary layer (LLBL) or ionosphere at 1000 km, whichever comes first. In this work, we define the LLBL at the magnetopause and the mantle at high latitudes where the field begins to have local minima. According to the Liouville's theorem the phase space density at this point at the $12 R_E$ boundary is equal to that where the particle starts. An initial proton distribution in the entire magnetosphere is needed to determine the distribution during the substorms. Table 1 lists models and satellite data we use for the initial ion distribution. Particles are released at $12 R_E$, at times = t_1 , t_2 , t_3 , t_4 , at 13 local times from 1300 to 0600 MLT along the nightside, 6 logarithmically spaced energies from 1.68 to 300 keV, 6 pitch angles from 7.5° to 82.5° , and 8 gyrophases from 0° to 315° . As a result, 14,976 particle trajectories are traced backward in time to their starting positions. No particle is released from the dayside because a mantle distribution (Table 1) is assumed there. Plate 1 plots the 14,976 initial particle locations of substorm 1 on the Z - X , X - Y , and Y - Z planes, with $+X$ corresponding to the antisunward direction. Color coding represents the ratio of final energy at $12 R_E$ to the initial energy. Most of the ions that lose energy (orange and red dots) start inside $12 R_E$. During the growth phase they drift radially outward to the $12 R_E$ boundary at t_2 . Particles that reach the $12 R_E$ boundary at t_3 and t_4 mostly come from the plasma sheet, lobes, mantle, or LLBL. They are energized when they are traveling radially inward to the inner plasma sheet in response to both steady convection and dipolarization. As shown in Plate 1, a notable portion of particles come from the mantle and LLBL. However, they do not contribute significantly to the hot plasma population at $12 R_E$ because there are few particles (very small phase space density) in these two regions in the appropriate energy range. The dominant phase space density contributions to the distributions at $12 R_E$ come from the plasma sheet and lobes. In the case of substorm 2, particles seen at the $12 R_E$ boundary generally come from

larger radial distances and thus experience stronger energization than those of substorm 1.

Figure 2 shows the calculated pitch-angle-averaged H^+ fluxes at five local times along the $12 R_E$ boundary at three different times during substorm 1 (top panels) and substorm 2 (bottom panels): beginning of growth phase (t_1), expansion onset (t_2), and immediately after dipolarization (t_3). In general, flux intensities are decreasing during the growth phase (t_1 to t_2) except at 2200 and 0000 MLT under strong convection. As the magnetosphere is expanding, particles are transported outward and deenergized. Ions with given energy seen at $12 R_E$ at t_2 came from the inner magnetosphere with higher initial energy. Since quiet-time energy spectra usually decrease with increasing energy, phase space densities at $12 R_E$ at t_2 are mapped to lower densities (higher energies) at earlier times. On the other hand, there are noticeable enhancements during dipolarization (t_2 to t_3). Using a similar argument, particles energized during substorm expansion originate from velocity space regions where particle phase space density is relatively large, namely at low energies in the source. In substorm 2 the tailward induced motion during the growth phase is more than compensated by the stronger convection. Not surprisingly, there is no significant substorm-associated flux depletion at 2200 and 0000 MLT. The plasma sheet flux dropouts and enhancements during substorms have been previously modeled using our single-particle code [*Sauvaud et al.*, 1996; *Delcourt and Sauvaud*, 1994].

3. Ring Current Development During Substorms

A bounce-averaged kinetic model of the ring current [*Fok and Moore*, 1997] is used to calculate the subsequent transport and trapping of the plasma sheet ions during the substorms. The H^+ distributions at $12 R_E$ calculated from the test-particle code are taken as boundary fluxes of the ring current model. An identical magnetic field model (Tsyganenko 89), convection electric field model (Volland), and initial ion distribution (Table 1) are applied in the ring current model as in the particle code. Loss due to charge exchange with neutral hydrogen along drift paths is included.

In Plate 2 we plot the pitch-angle-averaged H^+ fluxes at the equator at t_1 , t_2 and t_3 during substorm 1 (top panels) and substorm 2 (bottom panels). The simulation domain is bounded by field lines with 45° and 70° invariant latitudes. Ion energy distribution is color coded as shown in the color wheel, following the concept of photon energies with red brightness

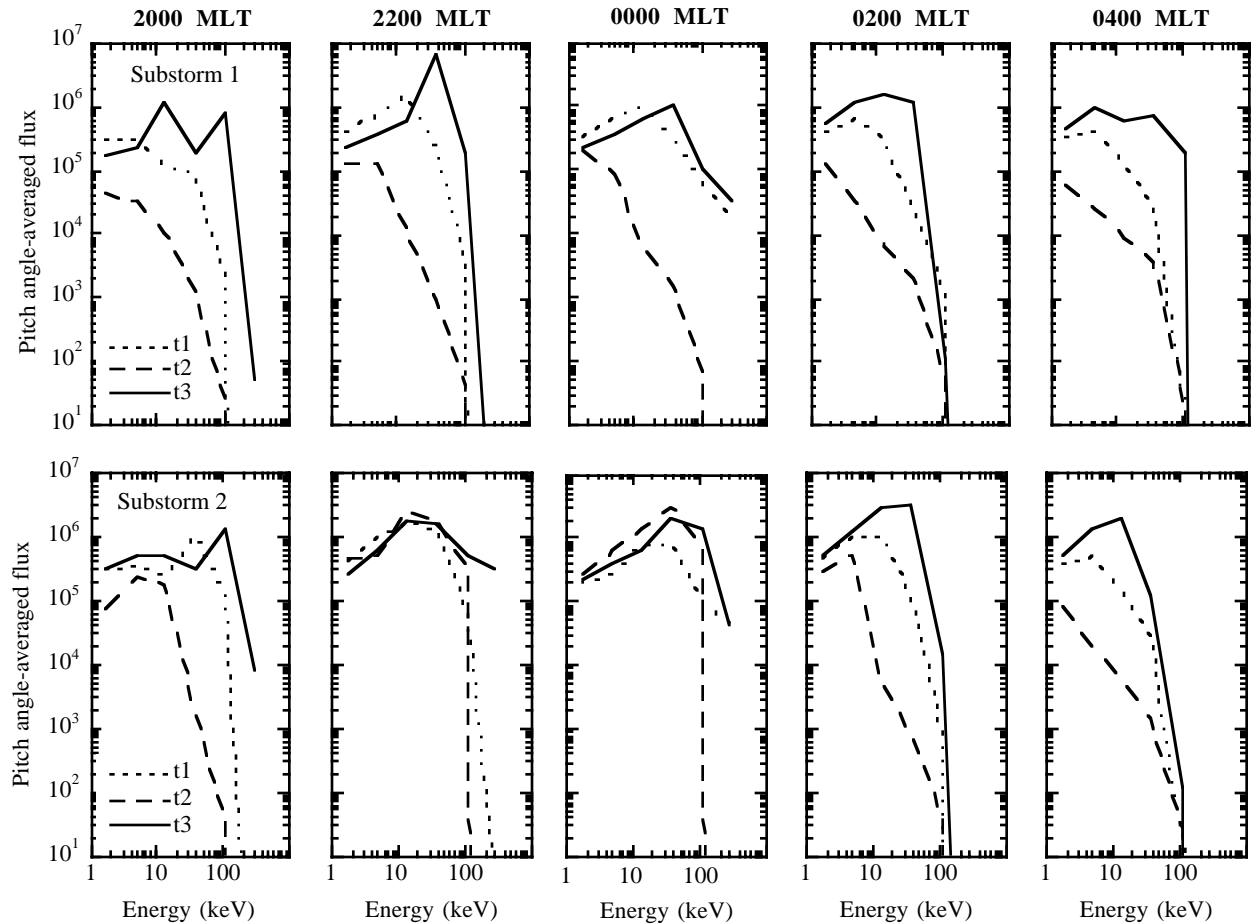


Figure 2. H^+ energy spectra at $12 R_E$, five magnetic local times, t_1 (dotted curves), t_2 (dashed curves), and t_3 (solid curves) as marked in Figure 1. Top panels show calculated fluxes during substorm 1 and bottom panels display fluxes in substorm 2.

representing low-energy (1–5 keV) flux, green representing medium-energy (5–40 keV) flux, and blue representing high-energy (40–300 keV) flux. In this representation, yellow signifies a spectrum dominated by low-energy and medium-energy particles with negligible contribution from high-energy particles. Similarly, cyan corresponds to distribution peaked toward high energies, and magenta to distribution peaked at high and low energies with a deficit at medium energy. Flux intensity is inferred by the brightness of color. White represents the average fluxes in all three energy ranges are above the flux scale limit, which is $10^6 \text{ cm}^{-2} \text{ s}^{-1} \text{ sr}^{-1} \text{ keV}^{-1}$ in Plate 2. It is sometimes difficult to resolve brightness from color; however, this is a useful tool to illustrate the spatial dependence of energy distribution.

As shown in Plate 2, the inner ring current is dominated by high-energy protons, whose charge exchange lifetime is long (days). As radial distance increases, the energy spectra before the substorm (at time t_1) are first dominated by high-energy particles, then by a combination of high-energy and low-energy particles (magenta), and finally, by a mix of low-energy and medium-energy particles (dim orange) in the outer region. The bright fringe on the nightside, in both cases, represents particles driven in by the steady convection.

During the growth phase, magnetic field lines are elongated and particles undergo betatron and Fermi deceleration. This deenergization is shown by the reddish color (low energy dominant) in the middle panels. However, in the case of strong steady convection (lower-middle panel), high particle fluxes are still seen in the premidnight sector at around $8 R_E$. From t_2 to t_3 the inflated magnetosphere collapses back to its original configuration (right panels). A broad area of enhanced fluxes suddenly appears on the nightside as the strong inductive electric field accelerates and transports particles earthward from the plasma sheet. When the freshly injected ions enter the region where azimuthal drifts are larger than earthward drifts, low-energy ions drift eastward and energetic ones drift westward. This particle diversion is reflected by the cyan color on the premidnight sector and yellow color on the postmidnight sector and is more obvious during substorm 2 than substorm 1. Immediately after expansion phase in substorm 2, the highest flux is located at ~ 2300 MLT at $6 R_E$, where dispersionless injection (white color, simultaneous injection at all energies) is seen.

As ring current particles are energized and deenergized during a substorm, the total energy carried by the ring current varies correspondingly, but in different locations for

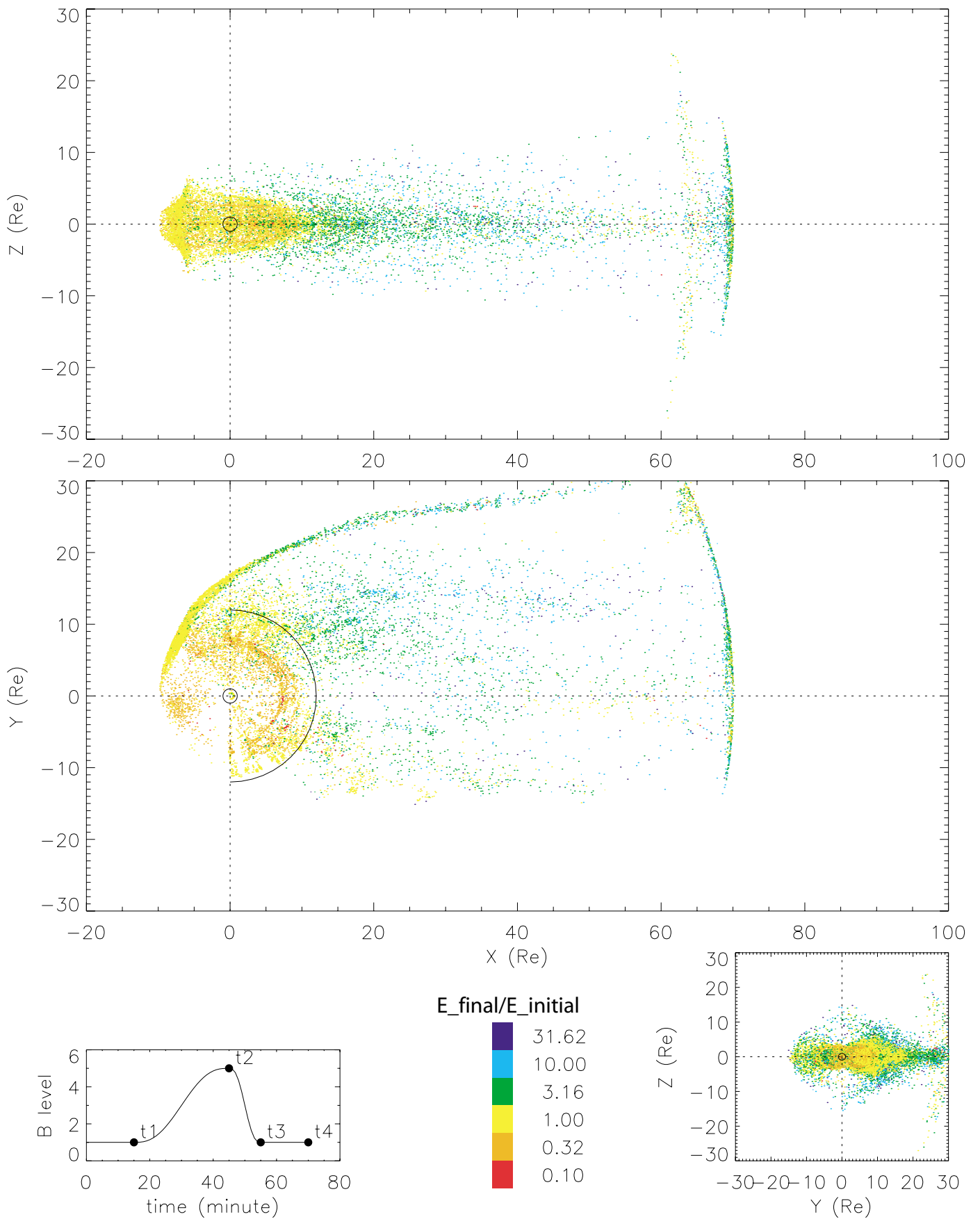


Plate 1. Starting locations, on Z–X, X–Y and Y–Z planes, of particles which arrive at 12 RE nightside boundary (black semicircle) at t1, t2, t3, and t4 during substorm 1. +X points antisunward. The ratio of final energy to initial energy is color coded.

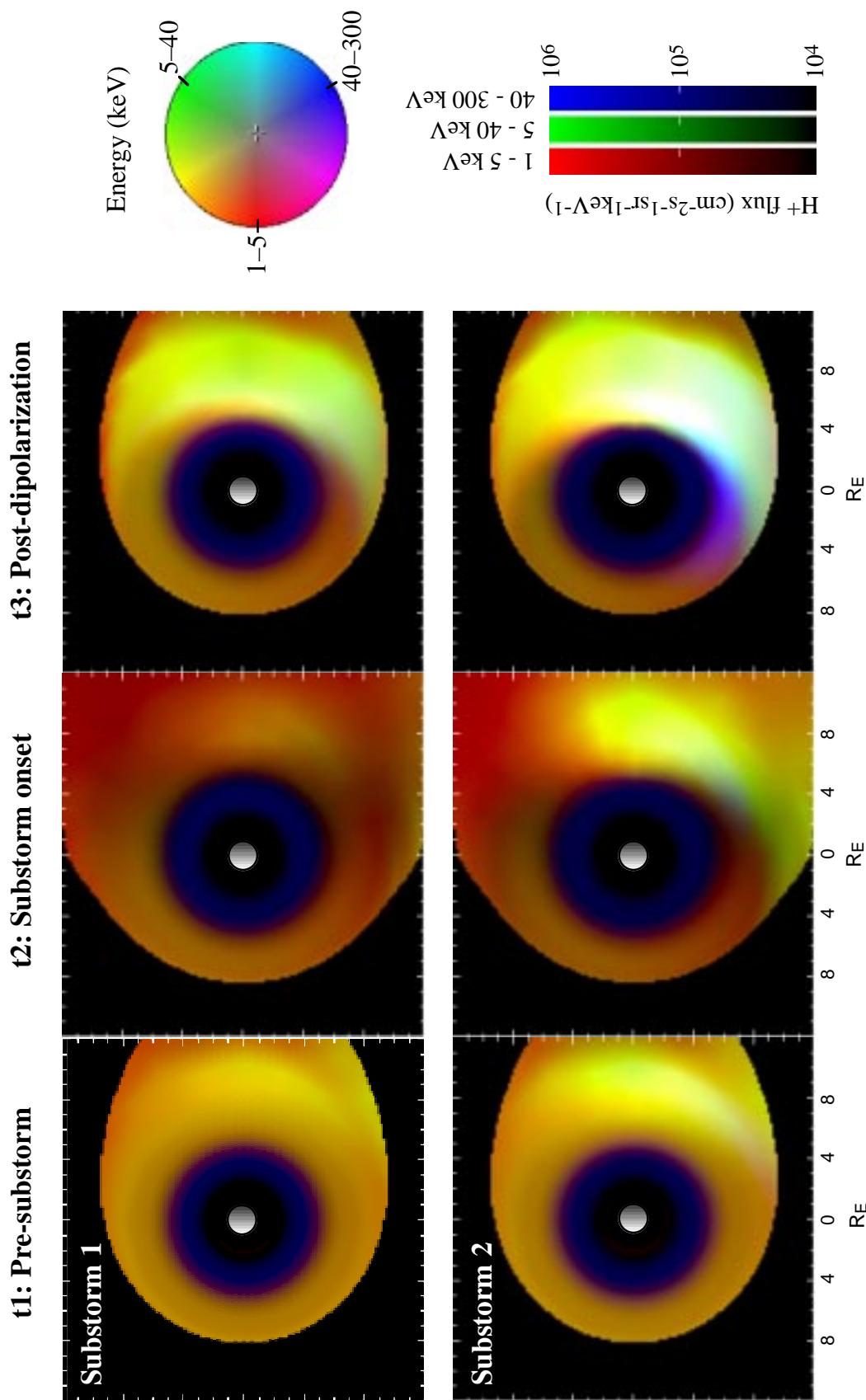


Plate 2. Pitch angle-averaged H^+ fluxes at the equator at t1, t2 and t3 (Figure 1) during substorm 1 (top panels) and substorm 2 (bottom panels). Ions with energies 1–5, 5–40 and 40–300 keV are represented by red, green and blue, respectively. The simulation region is between 45° to 70° invariant latitudes.

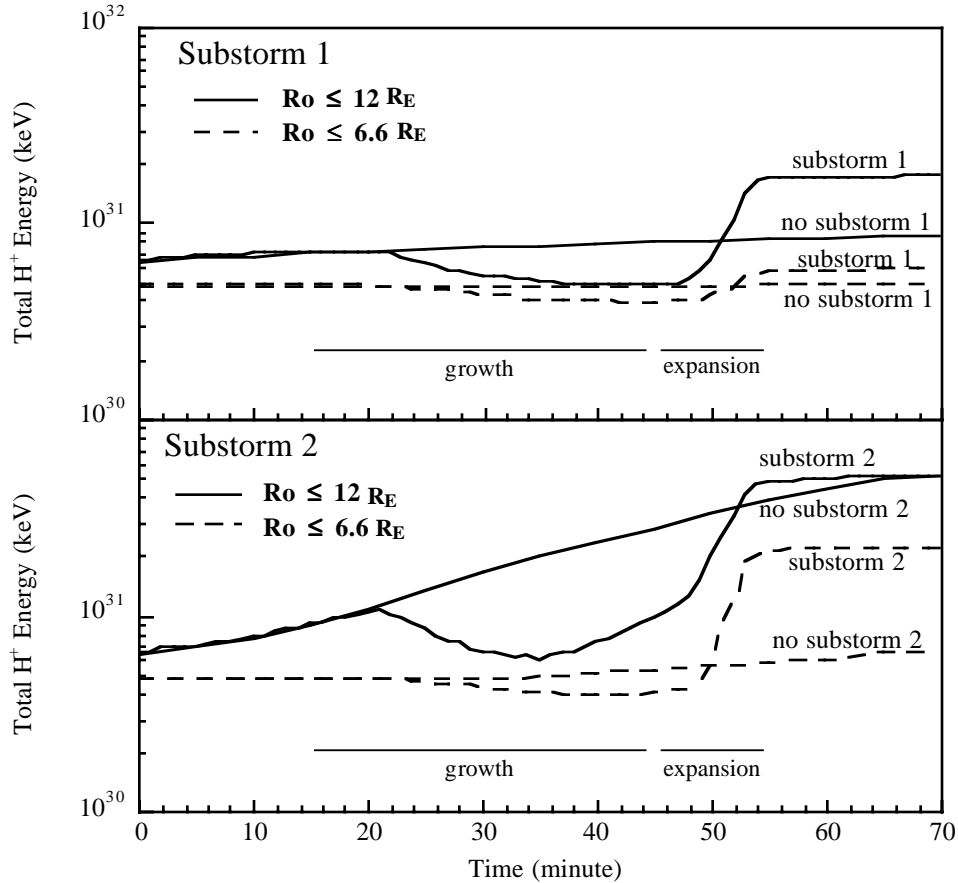


Figure 3. Total H^+ energy within $12 R_E$ (solid curves) and $6.6 R_E$ (dashed curves) during the two substorms. Also shown are total energies in the cases of no substorm cycle but only steady convection.

nonstorm and storm cases. We calculate, during the two substorms, the total energy of protons within $12 R_E$ (including inner plasma sheet) and within $6.6 R_E$ (inner magnetosphere only). The results are plotted in Figure 3, with and without the substorm cycle for each level of convection. During the stretching of the magnetosphere the energy content decreases in all cases. The ring current energy then rises sharply during dipolarization in all cases, except for the nonstorm inner magnetosphere. Relative to the curves describing the energy in the absence of a substorm cycle, there is significant net energy gain in the inner plasma sheet in the nonstorm case and in the inner magnetosphere for the storm case. Thus substorms occurring without a convection enhancement produce mainly an enhancement of the cross-tail current but little change in the ring current. The role of substorms in substorm 2 is to redistribute the plasma pressure closer to the Earth such that the resultant current distribution becomes more day-night symmetric. Strong convection by itself is not sufficient to push particles, especially high-energy particles, deep into the inner magnetosphere. However, dipolarizations together with strong convection can bring plasma sheet ions well inside the geosynchronous orbit and form a robust ring current. Our results suggest that substorm dipolarizations serve to enhance the penetration of the cross-tail potential deep into the inner magnetosphere and cause an efficient earthward transport of plasma sheet particles [Spiro *et al.*, 1988; Anderson *et al.*, 1993].

4. Shape and Propagation of Injection Boundary

The injection boundary has been defined as the earthward boundary of dispersionless plasma injection [McIlwain, 1974; Konradi *et al.*, 1975]. Signatures of the injection boundary are reproduced in our simulation. As shown in Plate 2, a broad area of enhanced fluxes is formed on the nightside during dipolarization and the intensities drop sharply on its earthward edge (right panels). To quantitatively identify the formation and propagation of this boundary at the equator, we construct an injection boundary as follows: We define a dispersionless injection as simultaneous enhancement of differential flux above $10^5 \text{ cm}^{-2} \text{ s}^{-1} \text{ sr}^{-1} \text{ keV}^{-1}$ in all three energy ranges (1–5, 5–40, 40–300 keV). When there is dispersionless injection, for a given local time, we locate the near-Earth point where the differential flux (averaged over both pitch angle and energy) drops to $1/\sqrt{e}$ of the maximum value. We define this location as the injection boundary at this particular local time if the subsequent two criteria are satisfied. First, the maximum flux at this local time has to be higher than $10^5 \text{ cm}^{-2} \text{ s}^{-1} \text{ sr}^{-1} \text{ keV}^{-1}$. Secondly, the intensity has to drop rapidly toward the Earth such that the distance between $1/\sqrt{e}$ and $1/e$ folding is less than $1 R_E$. Following these patterns, the "injection boundary" (white curves highlighted by black dots) at every 2 min during the expansion phase (from t_2 to t_3) is depicted in Plate 3. The geosynchronous orbit is also shown as a spatial reference. In substorm 1, dispersionless injection suddenly appears on the

nightside at 8 min after t_2 . As the magnetosphere continues to relax, the injection boundary moves earthward and expands from 2000 to 0300 MLT. For substorm 2, enhanced fluxes at "all" energies begin to be seen at 2 min after t_2 just outside the geosynchronous orbit in the premidnight sector. Four minutes later, the injection boundary moves inside the geosynchronous orbit around midnight and extends further in local time from 1800 to 0200 MLT. At t_3 the injection region spreads azimuthally to 1600 MLT and earthward to $\sim 5.3 R_E$ at 0000 MLT. We estimate that the earthward propagation velocity of this injection front is ~ 13 km/s and the azimuthal expansion is ~ 100 km/s. The rates of propagation of this injection front are consistent with that reported by *Moore et al.* [1981] and *Jacquey et al.* [1993].

The shape of the injection boundary has been proposed by many researchers. *McIlwain* [1974] performed particle trajectories tracing from the time of their encounter with the ATS-5 satellite backward to the substorm onset time. They found a spiral-shaped inner boundary of injection. *Mauk and Meng* [1983] imposed a double-spiraled injection boundary and were able to reproduce various dispersion patterns frequently observed by geostationary satellites. *Birn et al.* [1997] analyzed a full year of data from a spacecraft in geosynchronous orbit. They found five classes of injections events: pure ion injection, ion injection followed by electron injection, simultaneous ion and electron injection, electron injection followed by ion injection, and pure electron injection. These five categories of events were found to be well order with respect to local time. *Birn et al.* suggested that injection boundaries for ions and electrons are not identical but are displaced from each other in the dawn-dusk direction. Our results, shown in Plate 3, are consistent with the findings of *Birn et al.* Because of the westward magnetic drift of ions, the ion injection boundary extends more toward dusk than toward dawn. We did a test run for electrons and find that the shape of electron injection boundary is very similar to that of ions but extends more toward dawn. We find the radial distance of the ion injection boundary (r_b) as a function of local time (ϕ) fits well with the following form:

$$\begin{aligned} r_b &= r_m + C_e(\phi - \phi_m)^2 && \text{for } \phi \text{ eastward of } \phi_m \\ r_b &= r_m + C_w(\phi - \phi_m)^2 && \text{for } \phi \text{ westward of } \phi_m \end{aligned} \quad (1)$$

where ϕ_m is the local time in hours where the injection boundary is closest to the Earth at $r_b = r_m$. For both substorms, we find $\phi_m = 0000$ MLT, $C_e = 0.13 R_E/h^2$. For substorm 1 with a cross-polar cap potential drop of 40 kV we have $r_m = 5.8 R_E$, $C_w = 0.05 R_E/h^2$, and for substorm 2 with a cross-cap potential of 80 kV, $r_m = 5.3 R_E$, $C_w = 0.01 R_E/h^2$. We predict that in the limiting case of very strong convection, C_w will diminish, making the west side of the ion injection boundary circular. In this case, injected particles are trapped and drift around in local time. Figure 4 plots the simulated ion injection boundary (open circles) right after dipolarization (t_3) in substorm 2 and the functional fit (solid curve) from (1). The dashed curve is the estimated electron injection boundary found to be well represented from reflecting the ion boundary at the noon-midnight meridian. As shown in the figure, we reproduce the regions of pure ion injection, two-species injection and pure electron injection, as observed by *Birn et al.* [1997].

Plate 3 not only shows the inner edge of the enhanced fluxes but also the expansion of the injection region. Substorm-associated injection is first seen around midnight at $1\text{--}2 R_E$

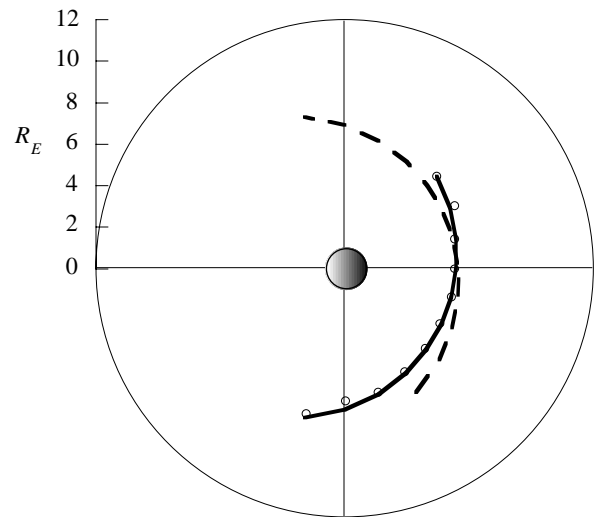


Figure 4. Ion and electron injection boundaries. Circles are simulation results for ions during a storm-time substorm. Solid curve is a fit for the calculation given by equation (1). Dashed curve is the assumed electron boundary.

outside the geosynchronous orbit, then expands in longitudinal, earthward, and tailward directions. The tailward boundary of the injection region has no sharp gradient but may be defined as the location of the 10^5 flux contour. The location of the tailward edge defined in this way moves from $\sim 2 R_E$ outside synchronous orbit out to $\sim 12 R_E$ in 6 min, corresponding a propagation rate of 70 km/s. The expansion of the dispersionless injection during substorm has been reported by *Lopez and Lui* [1990] using multisatellite observations. They associated this spatial evolution of plasma sheet with the spread of the substorm current wedge, which began to form in the near-geosynchronous region, and then expanded tailward as well as longitudinally. The formation of the substorm current wedge is not modeled in this work but is implicit in the dipolarization of the magnetic field. The expansion of injection region predicted here is a combined effect of earthward and azimuthal drifts and local energization of particles during dipolarization. Because of the global nature of the way we simulate a dipolarization event, we may overestimate the size of the injection region, especially in the azimuthal direction.

5. Substorm Injection Observed at Geosynchronous Orbit

As shown in Plates 2 and 3, our model generates substorm features such as dispersionless injection and the propagation of an injection front forming an injection boundary. Next we examine whether our calculation produces other signatures seen at the geosynchronous orbit during substorms. Figure 5 shows the simulated energy-time spectrograms of H^+ fluxes during substorm 1 (left panels) and substorm 2 (right panels) measured by five virtual geosynchronous satellites, which are separated by 3 hours and initially at local times spanning from 1500 to 0300 LT. The instantaneous magnetic configuration is plotted again at the bottom panels. In the first 20 min of steady convection the geosynchronous fluxes do not vary

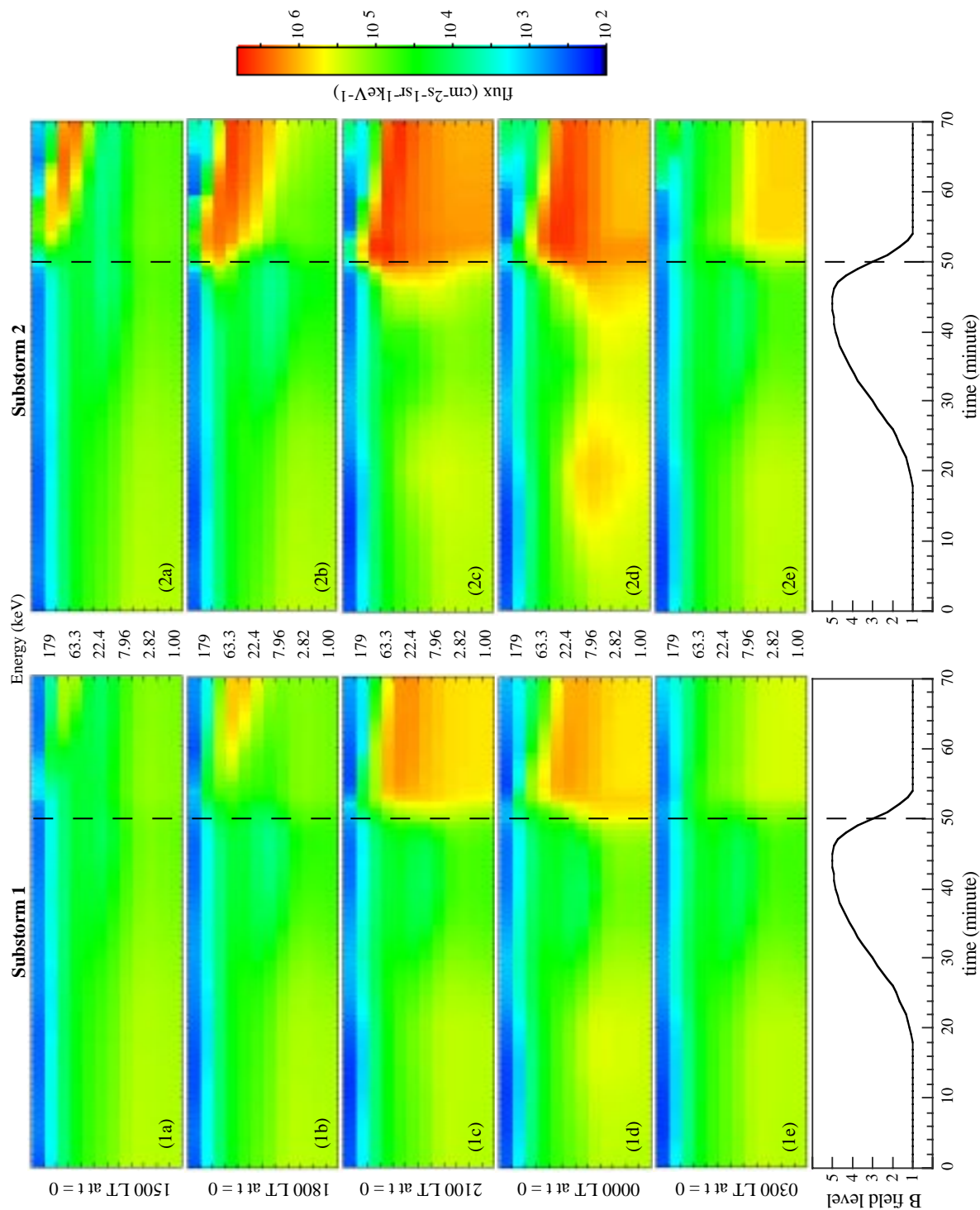


Figure 5. Simulated H⁺ fluxes along five virtual geosynchronous orbits, spread at 3 hour intervals in local time, during substorm 1 (right panels) and substorm 2 (left panels). Bottom panels are the modeled Tsyganenko magnetic field model level as a function of time. The dashed lines indicate the time at the middle of dopolarization (time = 50 minutes).

noticeably. However, near midnight, in the case of strong convection (panel 2d), a significant buildup of fluxes around 10 keV is seen.

During the growth phase from 20 to 45 min, flux dropouts are seen at almost all energies except ions with energies of 100s of keV, which are relatively uninfluenced by the induced electric field of the growth phase. At ~ 42 min when the elongation of the magnetosphere almost ceases, the enhanced fluxes due to convection appear again in the midnight sector. During substorm expansion at ~ 50 min, dispersionless injection is seen in the premidnight sector at 2100 to 0000 LT. A few minutes later, these freshly injected ions are dispersed by the Earth's magnetic field. Corotation dominates the motion of low-energy ions and they drift eastward toward dawn (panels 1e and 2e). High-energy ions drift westward to dusk and the more energetic ones lead the less energetic ones (panels a, b). No enhancement is found for ions with energies ≥ 150 keV, implying that the plasma sheet cannot supply particles of such high energies. This feature may correspond to the upper energy cutoff of plasma injection [Baker *et al.*, 1979]. The characteristics of geosynchronous fluxes during the two substorms are generally similar, although ion intensities are higher in substorm 2.

Dispersionless ion injection and flux dropout during substorms are frequently observed by satellites at the geosynchronous orbit [Mauk and Meng 1983; Baker and McPherron, 1990]. Actually, these particle signatures at $6.6 R_E$ are always used to identify substorm phases. The very distinct features seen at satellites at different local times, produced from our simulation, are consistent with previous observational and theoretical studies [i.e., Deforest and McIlwain, 1971; Mauk and Meng, 1983]. For example, the "tip" features in panels a and b in Figure 5 correspond to traces A and B of Deforest and McIlwain [1971, Figure 3], and the injection patterns shown in panels c and d are similar to those in "region 1" defined by Mauk and Meng [1983].

6. Discussions

We have tracked particles backward in time until they either exited the far plasma sheet (beyond $70 R_E$), or entered the HLBL (mantle) or LLBL (when they approach the magnetopause). Since we have only considered an isolated substorm cycle of 70 min, particles that backed out of the plasma sheet with low energies in the lobes were not tracked all the way to their probable ionospheric sources but were assigned phase space densities from representative distant plasma sheet populations. During this process, we found that while many trajectories originated in the boundary layers, they generally originated in regions of velocity space that contained negligible phase space densities, thereby making correspondingly negligible contributions to the density or pressure of plasma at the $12 R_E$ boundary.

We have not implemented a model of how or where the dipolarization is initiated nor of how it spreads within the magnetotail. Rather, we have used a model that invokes the dipolarization simultaneously throughout the modeled space, equivalent to the assumption that time for fast mode wave propagation throughout the magnetotail is much shorter than substorm timescales. This is clearly a limitation in the realism of our simulation insofar as fast mode propagation delays are comparable to the timescales of the substorm phenomenon. It

has been suggested that dipolarization occurs rapidly at some intermediate range in the tail and is subsequently communicated earthward by a compressional fast mode wave [Moore *et al.*, 1981] and tailward by an expansion fan wave [Jacquey *et al.*, 1993]. Fast mode waves propagate at over 1000 km/s throughout the regions of low plasma density but will slow down in the inner magnetosphere where the density rises rapidly [Moore *et al.*, 1981]. One shortcoming of our simulation results that may be suggestive of wave propagation effects is the relatively long timescale of injection events at the geosynchronous virtual spacecraft. The flux increase risetimes are a few to several minutes in duration at the fastest, whereas actual observations show risetimes as short as a few seconds [Moore *et al.*, 1981]. This suggests that compressional effects may be important at the inner edge of the plasma sheet, steepening the gradients even more than in our simulation results. It appears that a self-consistent model describing wave propagation will be needed to fully address the effects of finite wave speeds in magnetotail dynamics.

This study is based entirely on specified geoelectric and geomagnetic fields, and no attempt has been made to alter the fields using the computed particle pressures. The fields we have used are empirically generated and therefore closely representative of average conditions in the magnetosphere. Since they do not represent well short-term and local variability of the fields, it is somewhat surprising how well our results reproduce both qualitative and quantitative features of substorm and storm injection processes. In particular, the field variations we used do not contain any propagating waves, but rather the magnetic field varies proportionately at all spatial locations simultaneously.

Because our focus is on the injection process that contributes to the ring current through geosynchronous orbit, we have neglected in this study to include O^+ ions in our calculations to date. However, both of our models are fully capable of tracking other ion species, and this is a logical step to be taken in the future.

The physical origin of dispersionless injections near geosynchronous orbit is clearly depicted by this simulation. The dipolarization electric field is localized in local time in the midnight sector. Consequently, the acceleration of plasma is greatest in that sector, though the peak is skewed somewhat toward evening (morning) by the magnetic drifts that the bulk of the plasma ions (electrons) experience. This would be less true if the dipolarization occurred on an even shorter timescale than we have used. Observations from within the dipolarizing region exhibit little energy dispersion, but observations made away from the dipolarizing region are dominated by the differential drift transport of ions as a function of their energies, which produces positive dispersion (high energies first) duskward of the injection region and negative dispersion (low-energy ions first) dawnward of the injection region. In the limit that the injection occurs in a time much shorter than the drift periods of the ions, the result is exactly as described by Mauk and Meng [1983] and by Mauk [1986].

7. Conclusions

In this paper, we have augmented our earlier studies of magnetic storm and substorm in two ways, motivated largely by the rather modest effects of dipolarization events in our earlier simulations [Fok *et al.*, 1996]. First, we have extended

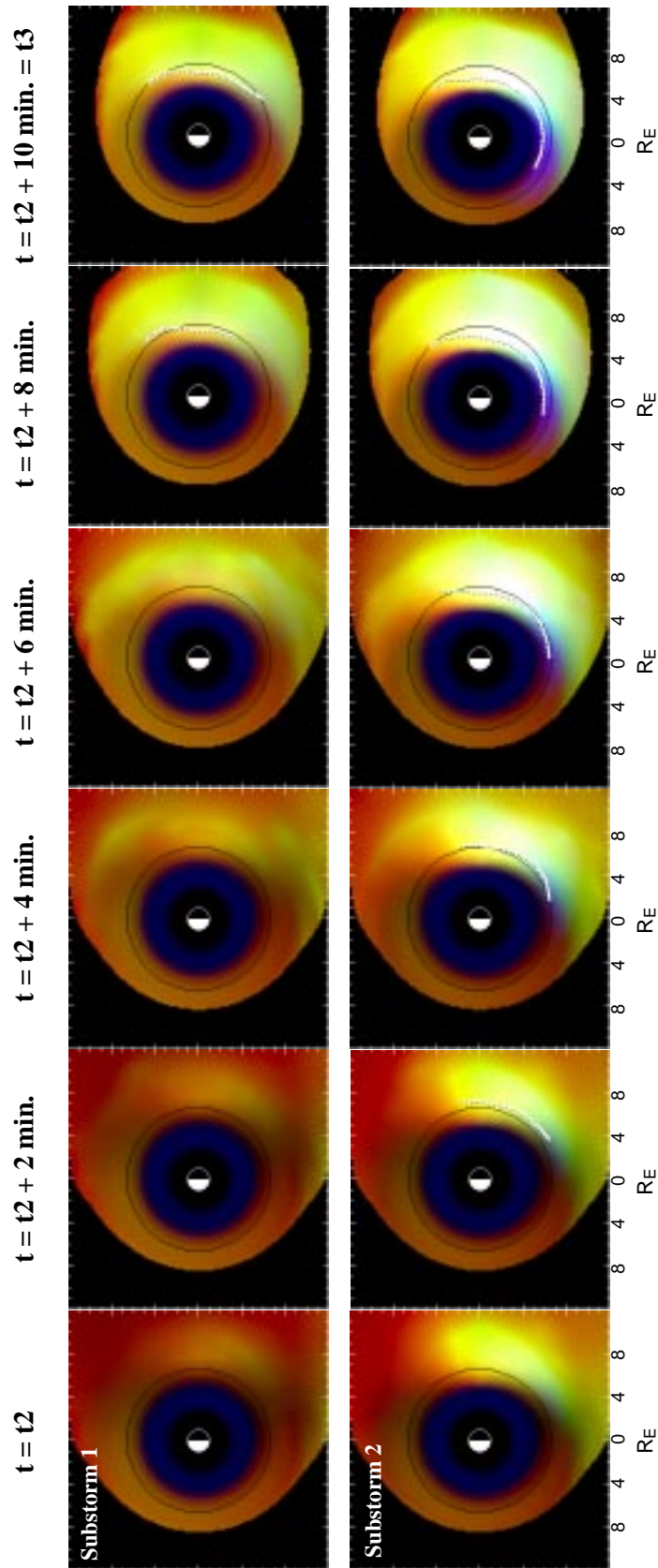


Plate 3. Injection boundaries (white curves highlighted by black dots) at the equator during expansion phase of substorm 1 (upper panels) and substorm 2 (lower panels). The black circles are geosynchronous orbits. Color scale is the same as Plate 2.

the range of the ring current model out to $12 R_E$ in the nightside magnetosphere. This allows for a boundary condition to be set well outside of geosynchronous orbit, at the outer limits of the region of validity of the adiabatic bounce-averaged ring current code. Secondly, we have modeled the ring current outer boundary plasma using a 3D test particle code to construct the ion velocity distribution there by backtracking particles from a representative velocity space grid to source regions assumed to have constant properties independent of the substorm/storm process. This provides a plasma to the inner region that is realistically influenced by dipolarization electric fields in the plasma sheet, in place of our earlier use of Active Magnetospheric Particle Tracer Explorers (AMPTE)/CCE observations (at 16 hours time resolution) to set the outer boundary condition for the ring current region.

We have assumed a globally-coherent dipolarization process, independent of any smaller-space or timescale phenomena that are part of it. Nevertheless, our simulations produce the main familiar features of substorm injection through the nightside geosynchronous orbit region. These conclusions are consistent with those of *Quinn and Southwood* [1982] and *Mauk* [1986], who previously asserted the importance of a "convection surge" and of the induced electric field associated with dipolarization of the magnetic field. To their studies, we have added nonadiabatic particle behavior in a three-dimensional simulation space and have thereby clarified the source of injected plasmas and the roles of global convection and individual substorms in generating the cross tail and ring currents. In the simulations we have reported on here, we find the following:

1. The major particle source of ion flux enhancements during substorms is freshly injected particles from the plasma sheet-lobe region.

2. An ion injection front is formed, which expands earthward in a rate of ~ 13 km/s, azimuthally in both directions in ~ 100 km/s and tailward in ~ 70 km/s, and these propagation rates are consistent with cited observations of substorm plasma expansion.

3. At the end of the expansion phase, the front stops moving after forming an ion injection boundary that is well represented by the functional form of equation (1), which is qualitatively similar in shape and location to that which has been reported in cited works. An electron boundary is also created with a shape similar to that of the ions but is shifted in local time. We have reproduced the regions of pure ion injection, ion-electron injection, and pure electron injection in a way that is qualitatively consistent with cited observations.

4. During the period after the substorm expansion phase, the simulated plasma ions are seen by virtual geosynchronous spacecrafts to disperse in local time in a way that is consistent with well-known patterns that have been shown to be produced by instantaneous injection boundary formation. These results suggest strongly that divergent reports of substorm propagation have been the result of differing spacecraft vantage points. Such observations seem to be well integrated by these modeling results.

5. Individual substorm dipolarizations create a significant enhancement of equatorial current density by redistributing plasma pressure earthward. During quiet times of weaker convection these enhancements mainly boost the cross-tail

current and stretch the tail. During storm periods of stronger convection the enhanced energy goes into the inner magnetosphere, boosting the ring current and inflating the magnetosphere.

Acknowledgments. We like to thank the two referees for their valuable comments. We are grateful for helpful discussions with R. A. Wolf, N. A. Tsyganenko, M. Hesse, B. L. Giles, and M. Goodman. For assistance with the chromogram true color displays, we are grateful to M. A. Sloan of Computer Sciences Corporation. This work was supported by the NASA Office of Space Science under UPN 432-20-00 and 344-14-10 and by grant NAG5-4968 to the Universities Space Research Association.

Janet G. Luhmann thanks Robert V. Hilmer and Xinlin Li for their assistance in evaluating this paper.

References

- Aggson, T. L., and J. P. Heppner, Observations of large transient magnetospheric electric fields, *J. Geophys. Res.*, **82**, 5155-5164, 1977.
- Anderson, P. C., W. B. Hanson, R. A. Heelis, J. D. Craven, D. N. Baker, and L. A. Frank, A proposed production model of rapid subauroral ion drifts and their relationship of substorm evolution, *J. Geophys. Res.*, **98**, 6069-6078, 1993.
- Arnoldy, R. L., and T. E. Moore, Longitudinal structure of substorm injections at geosynchronous orbit, *J. Geophys. Res.*, **88**, 6213-6220, 1983.
- Baker, D. N., and R. L. McPherron, Extreme energetic particle decreases near geostationary orbit: A manifestation of current diversion within the inner plasma sheet, *J. Geophys. Res.*, **95**, 6591-6599, 1990.
- Baker, D. N., R. D. Belian, P. R. Higbie, and E. W. Hones Jr., High-energy magnetospheric protons and their dependence on geomagnetic and interplanetary conditions, *J. Geophys. Res.*, **84**, 7138-7154, 1979.
- Bilitza, D., K. Rawer, L. Bosny, and T. Gulyaeva, International reference ionosphere—Past, present, future, *Adv. Space Res.*, **13**(3), 3-23, 1993.
- Birn, J., M. F. Thomsen, J. E. Borovsky, G. D. Reeves, D. J. McComas, and R. D. Belian, Characteristic plasma properties during dispersionless substorm injections at geosynchronous orbit, *J. Geophys. Res.*, **102**, 2309-2324, 1997.
- Chen, M. W., L. R. Lyons, and M. Schulz, Simulations of phase space distributions of storm time proton ring current, *J. Geophys. Res.*, **99**, 5745-5759, 1994.
- DeForest, S. E., and C. E. McIlwain, Plasma clouds in the magnetosphere, *J. Geophys. Res.*, **76**, 3587-3611, 1971.
- Delcourt, D. C., and J. A. Sauvaud, Plasma sheet ion energization during dipolarization events, *J. Geophys. Res.*, **99**, 97-108, 1994.
- Delcourt, D. C., J. A. Sauvaud, and A. Pedersen, Dynamics of single particle orbits during substorm expansion phase, *J. Geophys. Res.*, **95**, 20,853-20,865, 1990.
- Fok, M.-C., and T. E. Moore, Ring current modeling in a realistic magnetic field configuration, *Geophys. Res. Lett.*, **24**, 1775-1778, 1997.
- Fok, M.-C., T. E. Moore, and M. E. Greenspan, Ring current development during storm main phase, *J. Geophys. Res.*, **101**, 15,311-15,322, 1996.
- Ganguli, S. B., The polar wind, *Rev. Geophys.*, **34**, 311-348, 1996.
- Gonzalez, W. D., J. A. Joselyn, Y. Kamide, H. W. Kroehl, G. Rostoker, B. T. Tsurutani, and V. M. Vasyliunas, What is a geomagnetic storm, *J. Geophys. Res.*, **99**, 5771-5792, 1994.
- Harel, M., R. A. Wolf, P. H. Reiff, R. W. Spiro, W. J. Burke, F. J. Rich, and M. Smiddy, Quantitative simulation of a magnetospheric substorm, I, Model logic and overview, *J. Geophys. Res.*, **86**, 2217-2241, 1981.
- Hesse, M., and J. Birn, Neutral atom imaging of the plasma sheet: Fluxes and instrument requirements, in *Measurement Techniques in Space Plasmas Fields*, *Geophys. Monogr. Ser.*, vol. 103, edited by R. F. Pfaff, J. E. Borovsky, and D. T. Young, pp. 297-304, AGU, Washington, D. C., 1998.
- Hughes, W. J., The magnetopause, magnetotail, and magnetic reconnection, in *Introduction to Space Physics*, edited by M. G.

- Kivelson and C. T. Russell, chap. 9, Cambridge Univ. Press, New York, 1996.
- Jacquey, C., J. A. Sauvaud, and J. Dandouras, Tailward propagating cross-tail current disruption and dynamics of the near-Earth tail: A multi-point measurement analysis, *Geophys. Res. Lett.*, *20*(10), 983, 1993.
- Konradi, A., C. L. Semar, and T. A. Fritz, Substorm-injected protons and electrons and the injection boundary model, *J. Geophys. Res.*, *80*, 543-552, 1975.
- Li, X., I. Roth, M. Temerin, J. Wygant, M. K. Hudson, and J. B. Blake, Simulation of the prompt energization and transport of radiation particles during the March 23, 1991 SSC, *Geophys. Res. Lett.*, *20*, 2423-2426, 1993.
- Li, X., D. N. Baker, M. Temerin, G. D. Reeves, and R. D. Belian, Simulation of dispersionless injections and drift echoes of energetic electrons associated with substorms, *Geophys. Res. Lett.*, *25*(20), 3763-3766, 1998.
- Liu, W. W., and G. Rostoker, Energetic ring current particles generated by recurring substorm cycles, *J. Geophys. Res.*, *100*, 21,897-21,910, 1995.
- Lopez, R. E., and A. T. Y. Lui, A multisatellite case study of the expansion of a substorm current wedge in the near-Earth magnetotail, *J. Geophys. Res.*, *95*, 8009-8017, 1990.
- Lopez, R. E., D. N. Baker, A. T. Y. Lui, D. G. Sibeck, R. D. Belian, R. W. McEntire, T. A. Potemra, and S. M. Krimigis, The radial and longitudinal propagation characteristics of substorm injections, *Adv. Space Res.*, *8*(9), 91-95, 1988.
- Lopez, R. E., D. G. Sibeck, R. W. McEntire, and S. M. Krimigis, The energetic ion substorm injection boundary, *J. Geophys. Res.*, *95*, 109-117, 1990.
- Mauk, B. H., Quantitative modeling of the "convection surge" mechanism of ion acceleration, *J. Geophys. Res.*, *91*, 13,423-13,431, 1986.
- Mauk, B. H., and C.-I. Meng, Characterization of geostationary particle signatures based on the "injection boundary" model, *J. Geophys. Res.*, *88*, 3055-3071, 1983.
- Mauk, B. H., and C.-I. Meng, Macroscopic ion acceleration associated with the formation of the ring current in the earth's magnetosphere, in *Ion Acceleration in the Magnetosphere and Ionosphere*, *Geophys. Monogr. Ser.*, vol. 38, edited by T. Chang, pp. 351-361, AGU, Washington, D. C., 1986.
- McIlwain, C. E., Substorm injection boundaries, *Magnetospheric Physics*, edited by B. M. McCormac, pp. 143-154, D. Reidel, Norwell, Mass., 1974.
- Moore, T. E., R. L. Arnoldy, J. Feynman, and D. A. Hardy, Propagating substorm injection fronts, *J. Geophys. Res.*, *86*, 6713-6726, 1981.
- Moore, T. E., et al., High-altitude observations of the polar wind, *Science*, *277*, 349-351, 1997.
- Ohtani, S., Earthward expansion of tail current disruption: Dual-satellite study, *J. Geophys. Res.*, *103*, 6815-6825, 1998.
- Quinn, J. M., and D. J. Southwood, Observations of parallel ion energization in the equatorial region, *J. Geophys. Res.*, *87*, 10,536-10,540, 1982.
- Sauvaud, J. A., T. Beutier, and D. Delcourt, On the origin of flux dropouts near geosynchronous orbit during the growth phase of substorms, 1, Betatron effects, *J. Geophys. Res.*, *101*, 19,911-19,919, 1996.
- Sheldon, R. B., and D. C. Hamilton, Ion transport and loss in the Earth's quiet ring current, 1, Data and standard model, *J. Geophys. Res.*, *98*, 13,491-13,508, 1993.
- Shepherd, G. G., R. Bostrom, H. Derblom, C.-G. Falthammar, R. Gendrin, K. Kaila, A. Korth, A. Pedersen, R. Pellinen, and G. Wrenn, Plasma and field signatures of poleward propagating auroral precipitation observed at the foot of the Geos 2 field line, *J. Geophys. Res.*, *85*, 4587-4601, 1980.
- Spiro, R. W., R. A. Wolf, and B. G. Fejer, Penetration of high-latitude-electric-field effects to low latitudes during SUNDIAL 1984, *Ann. Geophys.*, *6*, 39-50, 1988.
- Tsyganenko, N. A., A magnetospheric magnetic field model with a warped tail current sheet, *Planet. Space Sci.*, *37*, 5-20, 1989.
- Volland, H., A model of the magnetospheric convection electric field, *J. Geophys. Res.*, *83*, 2695, 1978.
- Wolf, R. A., J. W. Freeman Jr., B. A. Hausman, R. W. Spiro, R. V. Hilmer, and R. L. Lambour, Modeling convection effects in magnetic storms, in *Magnetic Storms*, *Geophys. Monogr. Ser.*, vol. 98, edited by B. T. Tsurutani et al., pp. 161-172, AGU, Washington, D. C., 1997.

M.-C. Fok, Universities Space Research Association, Mail Code 692, NASA Goddard Space Flight Center, Greenbelt, MD 20771. (fok@gsfc.nasa.gov)

D. C. Delcourt, Centre d'étude des Environnements Terrestre et Planétaires, Centre National de la Recherche Scientifique, 4 Avenue de Neptune, Saint-Maur des Fosses, 94107, France. (delcourt@cetp.ipsl.fr)

T. E. Moore, Interplanetary Physics Branch, Mail Code 692, NASA Goddard Space Flight Center, Greenbelt, MD 20771. (thomas.e.moore@gsfc.nasa.gov)

(Received August 24, 1998; revised November 23, 1998; accepted January 4, 1999.)